Surface science approach of MnO-CeO_x(111) mixed oxide

Elfrida Ginting*
Department of Chemistry, Faculty of Mathematics and Natural Sciences, Universitas Negeri Medan, Medan 20221, Indonesia
*Email: elfridaginting@unimed.ac.id

Received 19 April 2021, Accepted 20 May 2021

Abstract *Ceria has unique abilities that makes it possible to be used as catalyst supports. The abilities of ceria are to store and release oxygen and easy transformation of Ce^{+4} to Ce^{+3} and vice versa Ceria as a catalyst support, showed a disadvantage over high temperature. The purpose of the paper is finding the right recipe for growing Mn-ceria mixed oxide. STM, XPS and LEED were used to acquire fundamental information. LEED experiments from Mn doped ceria mixed oxide specified that the films is well ordered. The LEED results is showing six spots that indicated the well ordered film and follow the (111) plane. Furthermore, for Mn doped ceria mixed oxide, there is no disctinct difference between higher stoichiometry and lower stoichiometry mixed oxide. But between higher and lower percentage of Mn, it has different structure. The triangle islands from higher Mn mixed oxide is MnO follow (111) plane. For both lower and higher Mn, oxygen vacancies can be recognized in reduced films.* [SURFACE SCIENCE APPROACH OF MNO-CEO_X(111) MIXED OXIDE] ***(J. Math. Nat. Sci., I(I): 10 - 20, 2021)***

***Keywords*:** *Mn-ceria, STM, XPS, LEED*

Introduction

There are many scientific research focus on ceria. Ceria has unique abilities that makes it possible to be used as catalyst supports. The abilities of ceria are to store and release oxygen and easy transformation of Ce^{+4} to Ce^{+3} and vice versa. Moreover, strong metal support interaction (SMSI) in ceria was gaining interest in the beginning of ceria papers (Trovarelli, 1996; Trovarelli, 2002). SMSI means ceria is an active support. Increasing in stability and reactivity of active metal are both of the effect of SMSI in ceria. Due to its aforementioned abilites, ceria has been used in many applications. The applications of ceria as a support for an active metals are ranging from biomedicine sensor (Sun et al., 2012), CO oxidation (Pozdnyakova et al., 2006; Tabakova et al., 2011a), water gas shift reaction (Fu et al., 2003; Tabakova et al., 2011b), reforming of alcohols (Senanayake et al., 2014), three way conversion in automobile (Gandhi et al., 2003; Kašpar et al., 2003), and solid oxide fuel cells (Liu et al., 2013; Lee et al., 2014). Cerium oxide belong to rare earth oxide. It has non magnetic and insulator properties. Ceria has a cubic fluorite crystal structure. In one unit cell, ceria contained four cerium atom and eight oxygen atom. According to experiment by Kummerle and co worker, lattice parameter of ceria is 5.411 Å (Heger, 1999). Among The most stable plane of ceria is (111). But recent results showed that other low index ceria such as (110) and (100) have higher reactivity (Nolan et al., 2005a; Nolan et al., 2005b). Due to ceria's insulator property, growing thin film of ceria is required for fundametal studies. Mullins et al. established a widely known recipe for growing epitaxial ceria thin film on Ru(0001) (Mullins et al., 1999). Ceria as a catalyst support, showed a disadvantage over high temperature. In order to make ceria more durable in high temperature, modification of ceria by doping with other metal is proposed. There are many results regarding modification of ceria with certain metal. Cu doped CeO_2 is synthesized using coprecipitation (Avgouropoulos et al., 2005). Sol-gel synthesis was performed to make $Ce_{0.9}Fe_{0.1}O_2$ (Liu et al., 2008). Pd-doped ceria can be produced using combustion synthesis and ultrasonic spray pyrolysis (Priolkar et al., 2002). All of the aforementioned results are conducted in the non clean laboratory. There are many unknown variables involves in the results. It is really important to excecute the investigation in the clean and UHV environment. Working in the

UHV environment will eliminate many unknown variables. There are also results related with the improvement of ceria by doping it with certain metal. For example, by inserting Zr or Pd, ceria will be more thermally stable and improve its OSC (Yang et al., 2006; Yang et al., 2007). There are also Pr and Sn doped into ceria (Zhang et al., 2008; Song et al., 2007), both of these dopant will help the reducibility of ceria at low temperature. Sc, Y, La are helping to improve the ion conductivity of ceria (Nakayama and Martin, 2009). Finally, similarly with Zr and Pd, Mn will help improve themal stability of ceria and enhance the OSC of ceria (Liang et al., 2008). Tang et al. (2010) found that the reducing energy for oxygen vacancy formation on Mn doped ceria are due to electronic modification and structural distortion. Mn doped ceria have been study for many applications. Vickers et al. have shown that Mn doped ceria oxide is an effective catalyst for methane oxidation (Vickers et al., 2015). Maintaining clean water is also application for Mn modified ceria (Larachi et al., 2002). There are many water pollutans such as ammonia, acetic acid, pyridine, phenol, and polyethylene-glycol can be oxidized with Mn doped ceria as the catalyst. The term for these reaction is wet oxidation. Other authors also mentioned the use of Mn doped ceria as catalyst for selective reaction of NO_x with NH_3 (Machida et al., 2000; Qi and Yang, 2003). For Zr modified ceria, it is clear that the improved reactivity is related with the formation of solid solution (Zhou et al., 2007; Shah et al., 2006). But for Mn modified ceria, it is still unclear whether the formation of solid solution is feasible or not.There are many literatures focus on Mn doped ceria. Most of the project related with theoretical studies and bench reaction. Fundamental studies conducting inside the UHV chamber are needed to fully comprehend the reason behind modification of ceria using Mn. There are two types of Mn doped ceria. The first type is Mn-ceria interfaces. Mn-ceria interfaces were made in two steps. Initially, Preparation of ceria thin film on Ru(0001) is conducted. The next step was dosing Mn at room temperature (Ginting et al., 2013; Ginting et al., 2016). The second type is Mn doped ceria mixed oxide. For the second type of Mn doped ceria, both Mn and ceria are simultaneously dose into the chamber. There are several findings related with Mn doped ceria mixed oxide. There are authors claimed the formation of $Ce_{0.9}Mn_{0.1}O_2$ despite there is no shift in lattice parameter (Kaneko et al., 2007). Observations of $Mn_{0.3}Ce_{0.7}O_x$ by Qi and Yang (2004) gave three main ideas. First, there are Mn_2O_3 phase separated from CeO_2 support. Second, strong interaction between Mn_2O_3 and CeO_2. Third, XRD indicated small shift in the lattice parameter of Mn doped ceria. Wu and co-worker concluded that catalytic activity of $Ce_{0.5}Mn_{0.5}O_2$ was due to the strong interaction between Mn and Ce. Despite of all the catalytic improvement of $Ce_{0.5}Mn_{0.5}O_2$, there is no shift in the lattice parameter of $Ce_{0.5}Mn_{0.5}O_2$ (Wu et al., 2007). XPS and STM studies of Mn doped ceria intefaces have been discussed by Zhou and group. Ginting and co worker explained that there are oxidation and reduction process between Mn and ceria. XPS results presented that by adding more Mn onto ceria, it will further reduced the ceria. Mn metallic is oxidized into Mn^{+2} (Ginting et al., 2013). STM studies for Mn modified ceria interface indicated the strong interaction between Mn and ceria (Ginting et al., 2016). There is no preferential landing for Mn. By annealing Mn on ceria interfaces at different temperature showed the stability of Mn on ceria. The height of Mn is stable eventhough it is annnealed to 800 K. Triangular domain is only observed for Mn on partially reduced at 800 K. It is concluded that sintering is not observed on Mn.This paper is focused on finding the right recipe for growing Mn-ceria mixed oxide. STM, XPS and LEED were used to acquire fundamental information. The project were conducted by varying the amount of Mn, oxygen pressure, and annealing time. LEED experiments verified that the mixed oxide is well ordered. The right recipe for growing Mn doped ceria mixed oxide were established. Eventhough it is not shown in the paper, there are only certain amount of Mn can be added into the ceria. Whenever percentage of Mn reached around 20%, there will be segregation of MnO from ceria. The segregation will have a triangular island with height around ~1 nm. The best results are mixed oxide with percentage of Mn below 10%.

Materials and Methods

All experiments in this study were performed on multitechnique UHV system manufactured by Omicron technology. Characterization and synthesis of sample of interest can be completed in the multitechnique UHV system. The base pressure of the multitechnique system is 5×10^{-11} Torr. The multitechnique UHV system consist of a variable temperature-scanning tunneling microscopy (VT STM XA650), 4-grid SPECTALEED optic, an EA 125 U1 hemispherical electron scpectrometer, quadrupole mass spectrometer (Hiden HAL/3F PIC), a DAR 400 twin-anode X-ray source, a manipulator with e-beam heater capabilities, and a metal evaporation sources. A Ru(0001) single crystal (Princeton Scientific Corp, diameter 10 mm, roughness < 0.03μ, orientation accuracy < 0.1º) was utilized as a substrate for the growth of Mn modified ceria mixed oxide. Ru(0001) crystal as a substrate will be cleaned with Ar ion sputtering (1 keV, 3 μA) followed by annealing to 1300 K for 45 s. STM, XPS and LEED were used to check whether Ru(0001) crystal is clean or not. Previous studies, Mn as a dopant was predeposited onto ceria. In this studies both Ce and Mn (Goodfellow, purity 99.98%) were deposited simultaneously. This method is an attempt to mimick the preparation of MnO-ceria mixed oxide. Both Ce and Mn metal source are homemade water-cooled electron beam evaporator. This studies is finding the right method for growing MnO-ceria mixed oxide. The flux of Ce is ~0.2 ML/min. Whereas the flux of of Mn is 0.04 ML/min. Adjusting oxygen pressure while growing MnO-ceria is also executed in this experiment. Previous studies indicated that modifying oxygen pressure will give different stoichiometry of ceria. XPS, STM, and LEED characterization were carried out at room temperature. All STM images were scanned using homemade etched Tungsten tip and completed in a constant current mode (sample bias: 1.0 V – 3.0 V; tunneling current: 0.05 nA-0.1 nA). STM measurements were performed using WxSM software (Horcas et al., 2007). XPS spectra were acquired using Mg Kα (1253.6 eV, 15 kV, 20 mA) with a fixed electron passing energy of 50 eV and an entrance slit size of 6×12 mm^2 in a high resolution scan mode. The spectra were recorded by using average two scans method. The final XPS spectra will have 0.02 eV steps. The calibration of XPS spectrometer was accomplished by scanning bulk Au foil (Alfa Aesar, 0.1 mm thick, 99.9975+%). The scanning is finalized by setting up binding energy of $4f_{7/2}$ at 84.0 eV. Ce 3d, O 1s, and Mn 2p are binding energies that will be monitored during this study. By monitoring all the aforementioned binding energies, the electronic properties of MnO-ceria can be understand. Finally, LEED experiments is using 80 eV beam energy.

Results

There are more than one trial employed for growing Mn doped ceria mixed oxide. Furthermore, all Mn doped ceria mixed oxide were grown with reactive deposition method. This means Mn and Ce were co-deposited in the presence of oxygen pressure onto Ru(0001) at 700 K. For all the sets, there are variation based on oxygen pressure, amount of Mn introduced, growth time and annealing temperature.The naming of each of Mn ceria mixed oxide were based on percentage of Ce, Mn and the stoichiometry. Percentage of Ce and Mn were determined by using similar method from Zhou and friends (Zhou and Zhou, 2010). The formula used to calculate the percentage of Mn in the mixed oxide is written below:

$$Mn\ (\%) = (I_{Mn}/S_{Mn})/(I_{Mn}/S_{Mn} + I_{Ce}/S_{Ce})$$

Where I is the integration of XPS peak after removing Shirley background and S is the atomic sensitivity factor (Wagner et al., 1981). The percentage of Ce^{+4} and Ce^{+3} were determined with peak fitting of Ce 3d region. The function used for the peak fitting is a mixed of Gaussian and Lorentzian functions and utilized fityk© for the XPS spectrum peak fitting. The naming of mixed oxide will be $Ce_{1-y}Mn_yO_{2-x}$ where y is the percentage of Mn and finally x is the loss of oxygen from fully oxidized ceria.The example of naming mixed oxide were started with the first trial. The first mixed oxide were grown using P_{oxygen} 8×10^{-8} Torr and growth time for 15 minutes followed by annealing the surface to 886 K. There are three main XPS spectrum scanned for the each mixed oxide that are Ce 3d, Mn 2p and O 1s. Integration of Ce 3d and Mn 2p area after subtracting Shirley background determined the value of I_{Mn} and I_{Ce}. From literature, sensitivity factor for Ce and Mn are 10 and 2.6 respectively (Wagner et al., 1981). Plug in all the values into equation 1 will give percentage of Mn equal to 18%. This is mean that percentage of Ce is equal to 82%. Peak decomposition of Ce 3d revealed the stoichiometry of ceria is 1.80. Hence, the mixed oxide name is $Ce_{0.82}Mn_{0.18}O_{1.80}$.

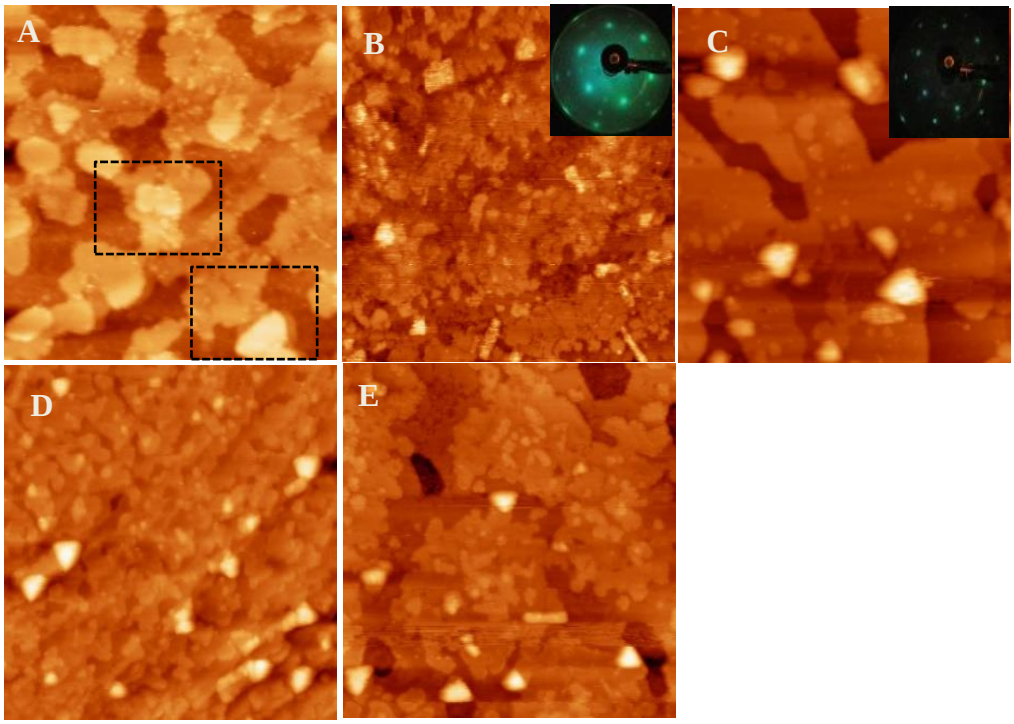

Figure 1. STM images of MnO ceria Mixed Oxide with higher percentage of Mn (A) $Ce_{0.82}Mn_{0.18}O_{1.80}$ annealed to 886 K (B) $Ce_{0.85}Mn_{0.15}O_{1.92}$ anneal to 778 K (C) $Ce_{0.85}Mn_{0.15}O_{1.92}$ anneal to 914 K (D) $Ce_{0.82}Mn_{0.18}O_{1.92}$ anneal to 778 K (E) $Ce_{0.82}Mn_{0.18}O_{1.92}$ anneal to 828 K. Inset for Figure 1C and 1D are their LEED images (Beam Energy: 60 eV).

Fig 1A presents STM image of $Ce_{0.82}Mn_{0.18}O_{1.80}$. There is no segregation observed in the film. eventhough the percentage of Mn is around 18%. $Ce_{0.82}Mn_{0.18}O_{1.80}$ films were grown layer by layer. There are no MnO triangle islands visible in the STM image. The reason is $Ce_{0.82}Mn_{0.18}O_{1.80}$ mixed oxide is only in submonolayer.

Height measurement for triple layer step region inside rectangle dash in Fig 1A are ranging from 0.37 nm Å and 0.63 nm. Likewise, the height of the most bright island (Dash circle in Fig 1A) is 0.61 nm. STM image of $Ce_{0.82}Mn_{0.18}O_{1.80}$ gives information related with the growth process, which is layer by layer mode. It is also interesting to observe STM image of $Ce_{0.82}Mn_{0.18}O_{1.80}$ since the film is continuous and relatively flat.Move on to spectroscopic results, Fig 2 displays comparison of Ce 3d spectrum from various Mn doped ceria with higher percentage of Mn. XPS spectra of Ce 3d region from $Ce_{0.82}Mn_{0.18}O_{1.80}$ film indicates higher percentage of Ce^{+3}, which is 39% . The percentage of Ce^{+3} correlated with the oxidation states of Mn. Fig 3 exhibits XPS spectrum of Mn 2p region from several mixed oxide.

Additionally, Fig 4 display O 1s peak fitting for $Ce_{0.85}Mn_{0.15}O_{1.92}$. There are two peaks can be positioned under O 1s. The first peak situated at 529.3 eV and the second peak located at 531.5 eV. Similar to those in first mixed oxide, the O 1s of $Ce_{0.85}Mn_{0.15}O_{1.92}$ indicated oxygen in ceria and surface oxygen The method for growing third mixed oxide is still executing reactive deposition. Both Ce and Mn introduced onto the Ru(0001) at 700 K in the presence 8×10^{-8} Torr oxygen for 25 min.

Fig 5A and 5B displayed STM images of $Ce_{0.96}Mn_{0.04}O_{1.90}$ on two different location. There is no triangle islands observed in Fig 5A and 5B. From these two results, it is concluded that the morphology of ceria MnO mixed oxide depend on the percentage of Mn. The formation of triangle island related with higher percentage of Mn. Fig 5A revealed flat and continuous surface. More dark protrusions are observed in the STM images. The height for bright island are around 0.20 nm. Whereas the depth for the dark protrusions are around 0.80 nm. Most of dark protrusion have a hexagonal shape. There are a few small dots present in the surface. Small dots in the surface correspond to the Ce atom adsorbed at the oxygen vacancies position i.e in the partially reduced ceria. In the same way with fourth mixed oxide, the fifth mixed oxide were prepared. The only difference is the amount of Mn introduced into the chamber. Percentage of Mn and Ce are 9% and 91% independently.

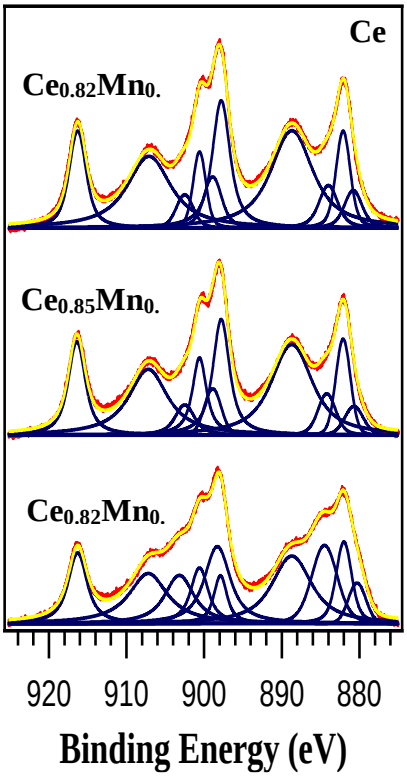

Figure 2. XPS Spectra of Ce 3d Region of MnO-Ceria Mixed Oxide with higher coverage of Mn .

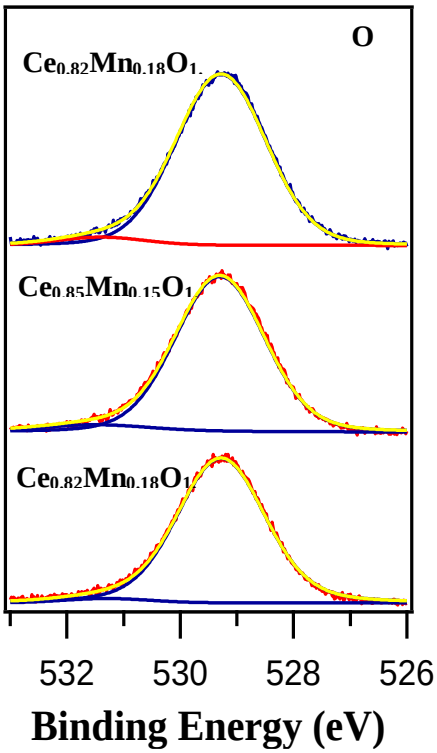

Figure 4. XPS spectra of O 1s Region of MnO Ceria Mixed Oxide higher percentage of Mn.

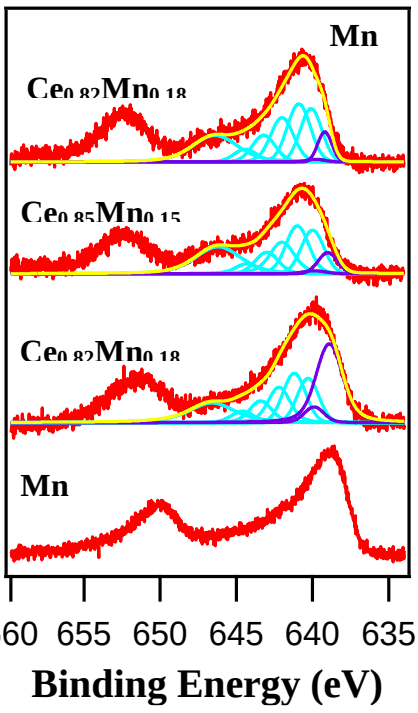

Figure 3. XPS Spectra of Mn 2p Region of MnO Ceria Mixed oxide with higher percentage of Mn.

In addition, stoichiometry of fifth mixed oxide is 1.92. Therefore the identity of fifth mixed oxide is $Ce_{0.91}Mn_{0.09}O_{1.92}$. Fig 5C and 5D represented STM image for $Ce_{0.91}Mn_{0.09}O_{1.92}$ on two different locations. With an increase of only 5% Mn, the triangle island is appeared again on the surface. The triangle islands have average height of 1.51 nm whereas the dark protrusion have average depth of 6.93 Å. In the same way with the fourth mixed oxide, $Ce_{0.91}Mn_{0.09}O_{1.92}$, also have dark small spots in the surface. Fig 2A inset exhibited LEED of Mn doped ceria. The LEED image indicated that doping Mn into ceria did not disturbed the (111) plane of the surface.

Discussion

XPS spectra Mn 2p region of $Ce_{0.82}Mn_{0.18}O_{1.80}$ points out that it has mixed Mn metallic and Mn^{+2}. The peak center for Mn $2p_{3/2}$ is 639.76 eV and double separation between Mn $2p_{3/2}$ and Mn $2p_{1/2}$ is 11.54 eV eV. Compared to Mn metallic NIST data base peak center for Mn $2p_{3/2}$ is 638.85 and 11.3 eV for splitting value (Naumkin et al., 2012). Additionally, XPS spectra for Mn 2p region of $Ce_{0.82}Mn_{0.18}O_{1.80}$ film is closer to Mn metallic. Peak fitting of Mn 2p region for $Ce_{0.82}Mn_{0.18}O_{1.80}$ showed

that there are 35.6% of Mn metallic and 64.4% of Mn^{+2}. Peak fitting method were conducted by following Biesinger and friends (Biesinger et al., 2011). All of these informations lead to a solid conclusion that $Ce_{0.82}Mn_{0.18}O_{1.80}$ film have mixed oxidation state i.e. Mn^{+2} and Mn^{0}. The results of mixed oxidation state of Mn is due to greater amount of Ce^{+3} and there is not enough oxygen in the surface to oxidize Mn completely into Mn^{+2}. Moreover, Barth and co worker performed peak fitting of O 1s using four Gaussian functions (Barth et al., 2016). Two peaks at 530.2 eV and 531.4 are identified as O-Ce^{+4} and O-Ce^{+3}, whereas the last two peaks at 532.6 eV and 533.3 eV correspond to hydroxyls joined with Ce^{+3} (Barth et al., 2016). Peak fitting of XPS spectrum of O 1s consisted of two peaks as shown in Fig 4. The first peak situated at 529.3 eV and the second peak is a shoulder peak centered at 531.3 eV. The first peak at 529.3 eV is corresponding to the oxygen in ceria whereas the shoulder peaks at 531.3 eV attributed to the defective oxides or surface oxygen. Peaks related with hydoxyls are not visible for O 1s spectra of $Ce_{0.82}Mn_{0.18}O_{1.80}$. The second mixed oxide were grown by using similar method with the first mixed oxide i.e. reactive deposition. The film started by co-deposited Ce and Mn at 700 K in the presence of 8×10^{-8} Torr oxygen for 25 min. The process is followed by subsequently annealing the film to 778 K and 914 K. In this second mixed oxide, there are growth time and annealing temperature variations. Using Equation 1, the percentage of Mn in the second mixed oxide is 15%. Then there is 85 % of Ce. Peak decomposition of Ce 3d indicated the stoichiometry of the mixed oxide is 1.92. Hence the name of second mixed oxide is $Ce_{0.85}Mn_{0.15}O_{1.92}$. STM images of $Ce_{0.85}Mn_{0.15}O_{1.92}$ annealed to 778 K present in Fig 1B whereas the STM images of $Ce_{0.85}Mn_{0.15}O_{1.92}$ annealed to 914 K exhibit in Fig 1C. The morphology of the mixed oxide annealed at different temperature are quite different. At 778 K, $Ce_{0.85}Mn_{0.15}O_{1.92}$ film have triangle islands that sit at the edge of the surface. The height of the triangle islands are in between 0.59 nm Å and 0.82 nm. Furthermore, there are also nano rods in the $Ce_{0.85}Mn_{0.15}O_{1.92}$ film with length in between 7.28 nm and 9 nm. The height for each of the nano rods is around 0.47 nm. Oxygen vacancies and nano lines can clearly be observed in the mixed oxide surface. There is no wide protrusion perceived in the lower annealing temperature mixed oxide.Utilization of LEED is required for checking whether the mixed oxide surface is well ordered. Beam energy for LEED is 80 eV. The inset is LEED images that represents $Ce_{0.85}Mn_{0.15}O_{1.92}$(111)p(2×1)-O. The hexagonal spots correspond with $Ce_{0.85}Mn_{0.15}O_{1.92}$(111) whereas the spots in between match with p(2×1) oxygen. The oxygen adsorption in the surface is due to low annealing temperature. Once, the annealing temperature is increased to 912 K, there is no more O adsorption on the surface. This can be confirmed with the LEED inset in Fig 1C. After annealing to 912 K, there are less spots in the p(2×1)-O. Fig 1C exhibits $Ce_{0.85}Mn_{0.15}O_{1.92}$ film annealed to 912 K. The morphology of the film changed after annealing process to higher temperature. There are bright wide protrusions noted in higher annealing temperature mixed oxide. In this set of experiment, the triangle islands have height in between 1.34 nm and 2.95 nm. The islands are also situated at the edge. Rectangle shape island is also perceived in the higher annealing temperature. The height for the rectangle shape island is 1.33 nm. In the wider region, there are many small islands with average height of 0.32 nm. There are no specific shape for the smaller islands. Higher annealing temperature and higher percentage of Mn affect the morphology of the mixed oxide. As can be seen in Fig 1B and 1C, the height of triangle island increased drastically corresponded to higher annealing temperature. STM result presents triangle islands in the mixed oxide. The triangular island in the surface is MnO that followed the (111) plane of ceria. Inset in Fig 1C is LEED of $Ce_{0.85}Mn_{0.15}O_{1.92}$ after annealing to 912 K. In the LEED result, there is still Ru(0001) and oxygen adlayer presents in the surface. This is due to lower annealing temperature. Fig 2 represents XPS spectra of Ce 3d for the mixed oxide with higher coverage of Mn. From XPS spectra, it can be seen that percentage of Ce^{+3} is around 16%. Furthermore, Fig 3 showed that Mn $2p_{3/2}$ peak center for $Ce_{0.85}Mn_{0.15}O_{1.92}$ shifted 1.8eV from Mn metallic state. Mn 2p region double splitting for $Ce_{0.85}Mn_{0.15}O_{1.92}$ is 11.82 eV. NIST data base for MnO double splitting is 11.60 eV and the peak center for Mn $2p_{3/2}$ is 640.4 eV (Naumkin et al., 2012). Hence, XPS spectra Mn 2p region for $Ce_{0.85}Mn_{0.15}O_{1.92}$ indicated that Mn^{+2} is the predominant species in the $Ce_{0.85}Mn_{0.15}O_{1.92}$. Peak fitting of Mn 2p region for $Ce_{0.85}Mn_{0.15}O_{1.92}$ concluded that the percentage of Mn^{0} is decreasing to 8.3 %. By reducing the amount of Mn in the mixed oxide, immediately the percentage of Mn^{0} is also reduced.

The process were followed by annealing the mixed oxide to 778 K and 828 K.In this set of experiment, the effect of annealing temperature on the morphology of mixed oxide is observed. The amount of Mn in the third mixed oxide is 18% and the percentage of Ce is 82%. Peak analysis of Ce 3d established 1.92 as stoichiometry value. Thus, the third mixed oxide label is $Ce_{0.82}Mn_{0.18}O_{1.92}$. Fig 1D exhibits STM image of $Ce_{0.82}Mn_{0.18}O_{1.92}$ annealed to 778 K. There are a few triangle island present in the $Ce_{0.82}Mn_{0.18}O_{1.92}$ at the edge of the terrace. The height of the triangle island is around 1.51 nm. Aside from triangle islands, the surface have height around 0.42 nm. Fig 1E showed STM image of $Ce_{0.82}Mn_{0.18}O_{1.92}$ after annealed to 828 K. The morphology of the surface is slightly changed. There are oxygen rows and surface defects appeared. Additionaly, there are around 5 triangle islands with average height of 1.54 nm and average length of 5.47 nm. Furthermore, there is one unique rod shape island in the surface. By comparing Fig 1D and 1E, it can be seen that there is no difference in height average between the two mixed oxide. The only obvious difference is oxygen row and surface defect is more define in Fig 1E. Additionally, there are lesser triangle island in Fig 1E compared to Fig 1D. Spectroscopy results will give an idea the electronic properties of the mixed oxide. Mn 2p spectra of $Ce_{0.82}Mn_{0.18}O_{1.92}$ were presented in Fig 3. The peak center for Mn $2p_{3/2}$ is 640.4 eV and the double splitting distance is 11.8 eV. These parameter indicated that Mn is predominantly in Mn^{+2} state. Percentage of Mn^{+2} in the mixed oxide can be determined using peak analysis. The peak fitting of Mn 2p region concluded that $Ce_{0.82}Mn_{0.18}O_{1.92}$ have around 7.5 % Mn metallic. Both $Ce_{0.85}Mn_{0.15}O_{1.92}$ and the $Ce_{0.82}Mn_{0.18}O_{1.92}$ have similar amount of Mn^{0}. Fig 4 revealed O 1s peak fitting for $Ce_{0.82}Mn_{0.18}O_{1.92}$. Both of the peak are located at 529.3 eV and 531.4 eV. There are no hydroxyl peaks visible in the peak analysis. Fig 1 represents STM images of ceria MnO mixed oxide with higher percentage of Mn. All mixed oxide have Mn with percentage above 15%. Triangle islands were presents in most of the mixed oxide with higher percentage of Mn. Next step will be comparison of STM results with lower percentage of Mn. In this case, it can be seen whether or not the triangle islands will be appeared in the mixed oxide. Fig 5 exhibits STM images of ceria MnO mixed oxide with lower percentage of Mn. The

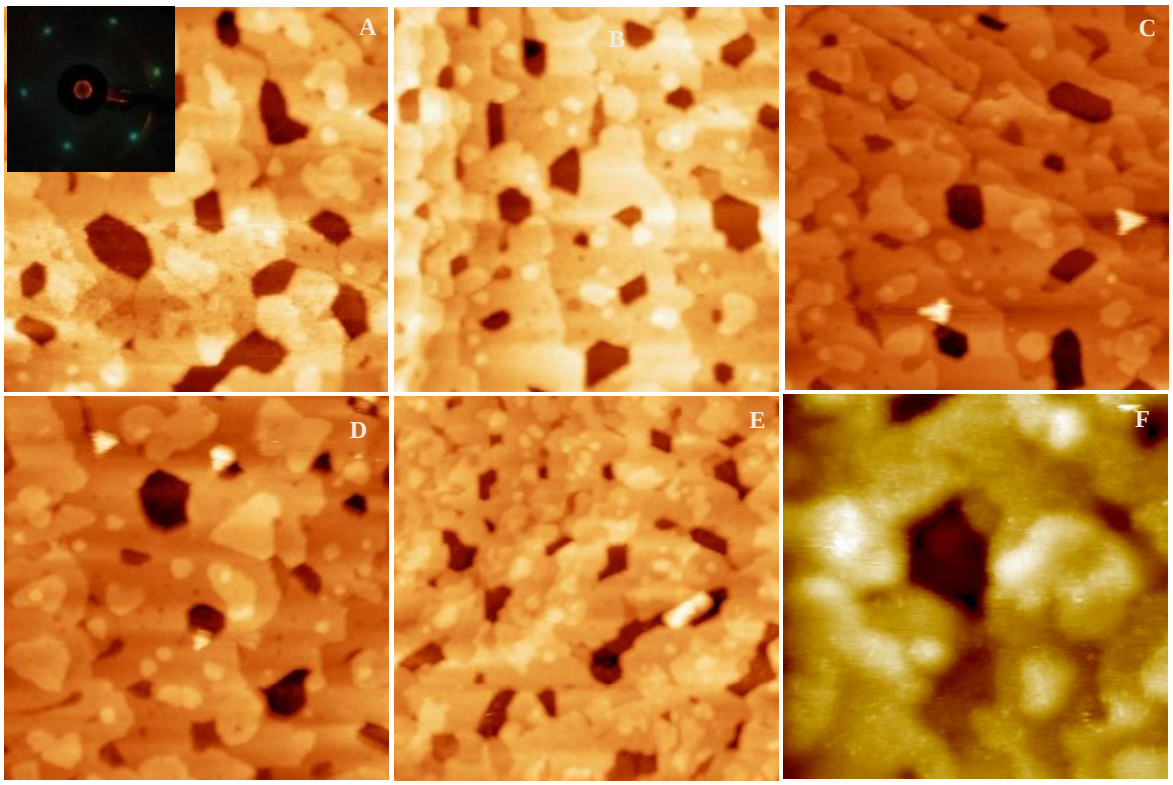

Figure 5. STM images of MnO Ceria Mixed Oxide with lower percentage of Mn (A) $Ce_{0.96}Mn_{0.04}O_{1.90}$ (B) $Ce_{0.96}Mn_{0.04}O_{1.90}$ at different region (C) $Ce_{0.91}Mn_{0.09}O_{1.92}$ (D) $Ce_{0.91}Mn_{0.09}O_{1.92}$ at different region. Inset is LEED image for $Ce_{0.96}Mn_{0.04}O_{1.90}$. (E) $Ce_{0.94}Mn_{0.06}O_{1.97}$ (F) $Ce_{0.94}Mn_{0.06}O_{1.97}$ at different location with image size 40 nm x 40 nm.

difference between Fig 1 and Fig 5 is the percentage of Mn in the surface. The fourth mixed oxide were made by co-deposited Ce and Mn at 700 K onto Ru(0001) at the presence of 8×10^{-8} Torr of oxygen. The process finalized by annealing the surface to 1150 K for 2 min. By implementing equation 1, percentage of Mn and Ce can be computed. Percentage Mn in fourth mixed oxide is 4%. Subsequently, the percentage of Ce is 96%. The stoichiometry of fourth mixed oxide is 1.92. Based from all the aforementioned parameter, the fourth oxide label is $Ce_{0.96}Mn_{0.04}O_{1.92}$.

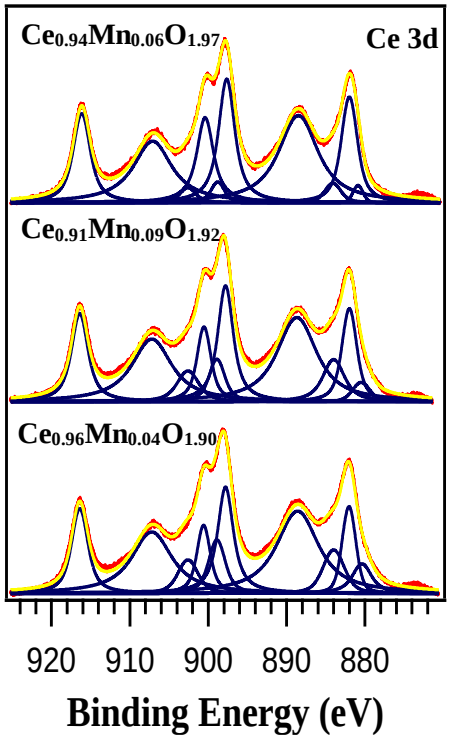

Figure 6. XPS Spectra of Ce 3d Region of MnO-Ceria Mixed Oxide with lower coverage of Mn.

The Mn ceria mixed oxide is well ordered. The sixth mixed oxide is also formulated using reactive deposition. The last trial is the only mixed oxide prepared with P_{oxygen} 2×10^{-7} Torr. There are 6% Mn and 94% Ce. In addition, the stoichiometry of sixth mixed oxide is 1.97. Consequently, the sixth mixed oxide designated as $Ce_{0.94}Mn_{0.06}O_{1.97}$ Fig 5E and 5F displayed STM images of $Ce_{0.94}Mn_{0.06}O_{1.97}$. From STM images of $Ce_{0.94}Mn_{0.06}O_{1.97}$, surface defect and oxygen vacancies are not clearly seen. The sixth mixed oxide is unique since all previous mixed oxide were grown using 8×10^{-8} Torr oxygen pressure.

There is no triangle island present in the surface since the percentage of Mn is around 6%. Also whenever the surface have higher oxygen in the surface, the STM images are not clear or slightly fuzzy. From previous group study, Mn ceria interfaces surface specified that there are reduction and oxidation process in the interaction. Similar phenomena happened with Mn doped ceria mixed oxide. Fig 6 revealed peak analysis of Ce 3d. The results indicated that $Ce_{0.96}Mn_{0.04}O_{1.90}$ have approximately 20% Ce^{+3}. Moreover, there are 15% Ce^{+3} on $Ce_{0.91}Mn_{0.09}O_{1.92}$. The lowest percentage of Ce^{+3} will be in $Ce_{0.96}Mn_{0.04}O_{1.97}$ which is 6%. All the aforesaid Ce^{+3} percentage can be interconnected with the percentage of Mn^{+2} in the mixed oxide. Fig 7 demonstrated Mn 2p peak fitting. $Ce_{0.96}Mn_{0.04}O_{1.90}$ have 5.2% Mn^{0} while $Ce_{0.91}Mn_{0.09}O_{1.92}$ have 6% Mn^{0}. Both of $Ce_{0.96}Mn_{0.04}O_{1.90}$ and $Ce_{0.91}Mn_{0.09}O_{1.92}$ have closer amount of Ce^{+3} which are 20% and 15% correspondingly. Furthermore, $Ce_{0.96}Mn_{0.04}O_{1.90}$ have Mn $2p_{3/2}$ peak at 640.1 eV and double splitting at 11.7 eV. Likewise, $Ce_{0.91}Mn_{0.09}O_{1.92}$ have Mn $2p_{3/2}$ peak at 640.6 eV and double splitting at 11.7 eV. Both of the number is really close to each other.

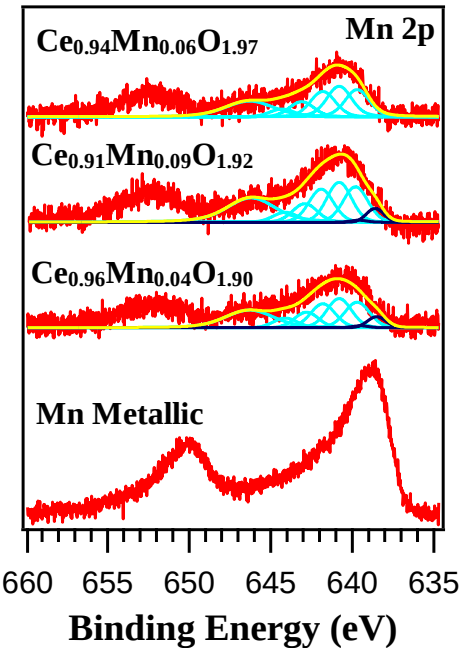

Figure 7. XPS Spectra of Mn 2p Region of MnO Ceria Mixed oxide with lower percentage.

All the aforementioned values indicate that both $Ce_{0.96}Mn_{0.04}O_{1.90}$ and $Ce_{0.91}Mn_{0.09}O_{1.92}$ have similar electronic properties. Finally, $Ce_{0.96}Mn_{0.04}O_{1.97}$ with lowest amount Ce^{+3} have 100% Mn^{+2}. Additionally, Mn 2p region for $Ce_{0.94}Mn_{0.06}O_{1.97}$ has double spliting at 11.9 eV and

Mn $2p_{3/2}$ peak centered at 640.6 eV. $Ce_{0.94}Mn_{0.06}O_{1.97}$ is the only mixed oxide that has 100% Mn^{+2}. This is due to lower amount of Mn introduced to the system and higher oxygen pressure used during the growth of $Ce_{0.94}Mn_{0.06}O_{1.97}$. Growing Mn doped ceria mixed oxide is possible in the UHV system. The percentage of Mn in the mixed oxide is crucial. Higher percentage of Mn in the surface resulted in the formation of MnO(111) triangle islands. The amount of oxygen introduced into the chamber will also affect the morphology of the surface. Surface defect and vacancies are more clearly seen in the partially reduced surface. Mixed Mn^{+2} and Mn metallic were found in most of the mixed oxide studied in this paper. But it is still possible to grow mixed oxide with 100% Mn^{+2}. Adjusting the amount of Mn and oxygen during the growth of mixed oxide film is the key to the number Mn species in the mixed oxide. Future work will be using Mn doped ceria mixed oxide as a support for Ni nanoparticles. It will be noteworthy to see whether the support will help stabilized the Ni nanoparticles.

Conclusion

The growth of Mn doped ceria mixed oxide is possible in the UHV system. XPS results indicated that oxidation states of Mn correlated with the amount of Mn and oxygen in the mixed oxide. Peak fitting of Mn 2p region signified that only mixed oxide grew using higher oxygen pressure have 100% Mn^{+2}. From all O 1s peak fitting, hydroxyls peaks is not visible. LEED experiments from Mn doped ceria mixed oxide specified that the films is well ordered. The LEED results is showing six spots that indicated the well ordered film and follow the (111) plane. The addition of other spots is match with p(2×1)-O adsorption. Once, the annealing temperature increased to 912 K, the spots in the p(2×1)-O is getting dimmer. Triangle islands with height above 1.0 nm. Once the percentage of Mn is reduced then triangle island is disappearing. The morphology of Mn doped ceria mixed oxide is totally different from Mn doped ceria interfaces. For Mn doped ceria interfaces, the morphology is depend on the stoichiometry of ceria. Whereas for Mn doped ceria mixed oxide, there is no disctinct difference between higher stoichiometry and lower stoichiometry mixed oxide. But between higher and lower Mn, it has different structure. The triangle islands from higher Mn mixed oxide is MnO follow (111) plane. For both lower and higher Mn, oxygen vacancies can be recognized in reduced films.

References

Avgouropoulos, G., Ioannides, T., Matralis, H. (2005) Influence of the preparation method on the performance of CuO–CeO2 catalysts for the selective oxidation of CO. *Appl. Catal. B: Environ.*, *56*(1-2): 87-93

Barth, C., Laffon, C., Olbrich, R., Ranguis, A., Parent, P., Reichling, M. (2016) A perfectly stoichiometric and flat CeO 2 (111) surface on a bulk-like ceria film. *Scient. rep.*, *6*(1): 1-6

Biesinger, M.C., Payne, B.P., Grosvenor, A.P., Lau, L.W., Gerson, A.R., Smart, R.S. C. (2011) Resolving surface chemical states in XPS analysis of first row transition metals, oxides and hydroxides: Cr, Mn, Fe, Co and Ni. *Appl. Surf. Sci.*, *257*(7): 2717-2730

Fu, Q., Saltsburg, H., Flytzani-Stephanopoulos, M. (2003) Active nonmetallic Au and Pt species on ceria-based water-gas shift catalysts. *Science*, *301*(5635): 935-938

Gandhi, H. S., Graham, G., McCabe, R. (2003) Automotive exhaust catalysis. *J. Catal.*, *216*(1-2): 433-442

Ginting, E., Hu, S., Thorne, J.E., Zhou, Y., Zhu, J., Zhou, J. (2013) Interaction of Mn with reducible CeO2 (1 1 1) thin films. *Appl. Surf. Sci.*, *283*: 1-5

Ginting, E., Peterson, E. W., Zhou, J. (2016) Scanning tunneling microscopy studies of Mn-doped CeOx (111) interfaces. *Appl. Catal. B: Environ.*, *197*: 337-342

Heger, E.A.K.A.G. (1999) The structures of C-$Ce_2O_{3+\delta}$, Ce_7O_{12}, ans $Ce_{11}O_{20}$. *J. Sol. Sta. Chem.*, *147*: 16

Horcas, I., Fernández, R., Gomez-Rodriguez, J.M., Colchero, J.W.S.X., Gómez-Herrero, J.W.S.X.M., Baro, A.M. (2007) WSXM: a software for scanning probe microscopy and a tool for nanotechnology. *Rev. Scient. Instr.*, *78*(1): 013705

Kaneko, H., Miura, T., Ishihara, H., Taku, S., Yokoyama, T., Nakajima, H., Tamaura, Y. (2007) Reactive ceramics of CeO2–MOx (M= Mn, Fe, Ni, Cu) for H2 generation by two-step water splitting using concentrated solar thermal energy. *Energy*, *32*(5): 656-663

Kašpar, J., Fornasiero, P., Hickey, N. (2003) Automotive catalytic converters: current status and some perspectives. *Catal. Today*, *77*(4): 419-449

Larachi, F., Pierre, J., Adnot, A., Bernis, A. (2002) Ce 3d XPS study of composite CexMn1− xO2− y wet oxidation catalysts. *Appl. Surf. Sci.*, *195*(1-4): 236-250

Lee, J.G., Park, J.H., Shul, Y.G. (2014) Tailoring gadolinium-doped ceria-based solid oxide fuel cells to achieve 2 W cm− 2 at 550 C. *Nat. Communicat.*, *5*(1): 1-10

Liang, Q., Wu, X., Weng, D., Xu, H. (2008) Oxygen activation on Cu/Mn–Ce mixed oxides and the role in diesel soot oxidation. *Catal. Today*, *139*(1-2): 113-118

Liu, C., Luo, L., Lu, X. (2008) Preparation of mesoporous Ce 1− x Fe x O 2 mixed oxides and their catalytic properties in methane combustion. *Kinet. Catal.*, *49*(5): 676-681

Liu, Z., Ding, D., Liu, M., Ding, X., Chen, D., Li, X., Xia, C., Liu, M. (2013) High-performance, ceria-based solid oxide fuel cells fabricated at low temperatures. *J. Pow. Sour.*, *241*: 454-459

Machida, M., Uto, M., Kurogi, D., Kijima, T. (2000) MnO x− CeO2 Binary Oxides for Catalytic NO x Sorption at Low Temperatures. Sorptive Removal of NO x. *Chem. Mat.*, *12*(10): 3158-3164

Mullins, D.R., Radulovic, P.V., Overbury, S.H. (1999) Ordered cerium oxide thin films grown on Ru (0001) and Ni (111). *Surf. Sci.*, *429*(1-3): 186-198

Nakayama, M., Martin, M. (2009) First-principles study on defect chemistry and migration of oxide ions in ceria doped with rare-earth cations. *Phy. Chem. Chem. Phy.*, *11*(17): 3241-3249

Naumkin, A.V., Kraut-Vass, A., Gaarenstroom, S.W., Powell, C.J. (2012) NIST standard reference database 20, version 4.1. *Nat. Inst. Stand. Technol. NIST, 1*: 1-49

Nolan, M., Grigoleit, S., Sayle, D.C., Parker, S.C., Watson, G.W. (2005a) Density functional theory studies of the structure and electronic structure of pure and defective low index surfaces of ceria. *Surf. Sci.*, *576*(1-3): 217-229

Nolan, M., Parker, S.C., Watson, G.W. (2005b) The electronic structure of oxygen vacancy defects at the low index surfaces of ceria. *Sur. Sci.*, *595*(1-3): 223-232

Pozdnyakova, O., Teschner, D., Wootsch, A., Kröhnert, J., Steinhauer, B., Sauer, H., Toth, L., Jentoft, F.C., Knop-Gericke, A., Paal, Z., Schlögl, R. (2006) Preferential CO oxidation in hydrogen (PROX) on ceria-supported catalysts, part II: Oxidation states and surface species on Pd/CeO2 under reaction conditions, suggested reaction mechanism. *J. Catal.*, *237*(1): 17-28

Priolkar, K.R., Bera, P., Sarode, P.R., Hegde, M.S., Emura, S., Kumashiro, R., Lalla, N.P. (2002) Formation of Ce1-x Pd x O2-δ Solid Solution in Combustion-Synthesized Pd/CeO2 Catalyst: XRD, XPS, and EXAFS Investigation. *Chem. Mat.*, *14*(5): 2120-2128

Qi, G., Yang, R.T. (2003) Performance and kinetics study for low-temperature SCR of NO with NH3 over MnOx–CeO2 catalyst. *J. Catal.*, *217*(2): 434-441

Qi, G., Yang, R.T. (2004) Characterization and FTIR studies of MnO x− CeO2 catalyst for low-temperature selective catalytic reduction of NO with NH3. *J. Phy. Chem. B*, *108*(40): 15738-15747

Senanayake, S.D., Mudiyanselage, K., Bruix, A., Agnoli, S., Hrbek, J., Stacchiola, D., Rodriguez, J.A. (2014) The unique properties of the oxide-metal interface: reaction of ethanol on an inverse model CeO x–Au (111) catalyst. *J. Phy. Chem. C*, *118*(43): 25057-25064

Shah, P.R., Kim, T., Zhou, G., Fornasiero, P., Gorte, R.J. (2006) Evidence for entropy effects in the reduction of ceria− zirconia solutions. *Chem. Mat.*, *18*(22): 5363-5369

Song, Z., Liu, W., Nishiguchi, H., Takami, A., Nagaoka, K., Takita, Y. (2007) The Pr promotion effect on oxygen storage capacity of Ce–Pr oxides studied using a TAP reactor. *Appl. Catal. A: Gen.*, *329*: 86-92

Sun, C., Li, H., Chen, L. (2012) Nanostructured ceria-based materials: synthesis, properties, and applications. *Energy Environ. Sci.*, *5*(9): 8475-8505

Tabakova, T., Avgouropoulos, G., Papavasiliou, J., Manzoli, M., Boccuzzi, F., Tenchev, K., Vindigni, F., Ioannides, T. (2011a) CO-free hydrogen production over Au/CeO2–Fe2O3 catalysts: Part 1. Impact of the support composition on the performance for the preferential CO oxidation reaction. *Appl. Catal. B: Environ.*, *101*(3-4): 256-265

Tabakova, T., Manzoli, M., Paneva, D., Boccuzzi, F., Idakiev, V., Mitov, I. (2011b) CO-free hydrogen production over Au/CeO2–Fe2O3 catalysts: Part 2. Impact of the support composition on the performance in the water-gas shift reaction. *Appl. Catal. B: Environ.*, *101*(3-4): 266-274

Tang, Y., Zhang, H., Cui, L., Ouyang, C., Shi, S., Tang, W., Li, H., Lee, J., Chen, L. (2010) First-principles investigation on redox properties of M-doped CeO 2 (M= Mn, Pr, Sn, Zr). *Phy Rev. B*, *82*(12): 125104

Trovarelli, A. (1996) Catalytic properties of ceria and CeO2-containing materials. *Catal. Rev.*, *38*(4): 439-520

Trovarelli, A. (2002) *Catalysis by ceria and related materials* (Vol. 2). World Scientific Publishing Co. Pte. Ltd., 5 Toh Tuck Link, Singapore 596224

Vickers, S.M., Gholami, R., Smith, K.J., MacLachlan, M.J. (2015) Mesoporous Mn-and La-doped cerium oxide/cobalt oxide mixed metal catalysts for methane oxidation. *ACS Appl. Mat. Interf.*, *7*(21): 11460-11466

Wagner, C.D., Davis, L.E., Zeller, M.V., Taylor, J.A., Raymond, R.H., Gale, L.H. (1981) Empirical atomic sensitivity factors for quantitative analysis by electron spectroscopy for chemical analysis. *Surf. Interf Anal.*, *3*(5): 211-225

Wu, X., Liang, Q., Weng, D., Fan, J., Ran, R. (2007) Synthesis of CeO2–MnOx mixed oxides and catalytic performance under oxygen-rich condition. *Catal. Today*, *126*(3-4): 430-435

Yang, Z., Woo, T.K., Hermansson, K. (2006) Effects of Zr doping on stoichiometric and reduced ceria: A first-principles study. *J. Chem. Phy.*, *124*(22): 224704

Yang, Z., Luo, G., Lu, Z., Hermansson, K. (2007) Oxygen vacancy formation energy in Pd-

doped ceria: A DFT+ U study. *J. Chem. Phy.*, *127*(7): 074704

Zhang, T.Y., Wang, S.P., Yu, Y., Su, Y., Guo, X.Z., Wang, S.R., Zhang, S.M., Wu, S.H. (2008) Synthesis, characterization of CuO/Ce0. 8Sn0. 2O2 catalysts for low-temperature CO oxidation. *Catal. Communicat.*, *9*(6): 1259-1264

Zhou, G., Shah, P.R., Kim, T., Fornasiero, P., Gorte, R.J. (2007) Oxidation entropies and enthalpies of ceria–zirconia solid solutions. *Catal. Today*, *123*(1-4): 86-93

Zhou, Y., Zhou, J. (2010) Growth and surface structure of Ti-doped CeO x (111) thin films. *J. Phy. Chem. Let.*, *1*(11): 1714-1720